Eur. Phys. J. D (2023) 77:57
https://doi.org/10.1140/epjd/s10053-023-00637-1

THE EUROPEAN PHYSICAL JOURNAL D

Regular Article – Clusters and Nanostructures

Multiple magnetic dipole excitation in permittivity-asymmetric all-dielectric metamaterials induced by quasi-bound states in the continuum

Meng Wang[1,a] and Wudeng Wang[2,b]

[1] Henan Province Engineering Research Center of Microcavity and Photoelectric Intelligent Sensing, School of Electronics and Electrical Engineering, Shangqiu Normal University, Henan 476000, China
[2] School of Mathematical and Physical Sciences, Dalian Polytechnic University, Dalian 116034, China

Received 13 December 2022 / Accepted 14 March 2023 / Published online 6 April 2023

Abstract. In this work, we numerically investigate multiple magnetic dipole (MD) excitation in an all-dielectric metamaterial of permittivity-asymmetric nanodisk dimer with symmetric geometric parameters. Besides the original MD mode, the permittivity-asymmetric metamaterials can support symmetry-protected dual quasi-bound states in the continuum (BICs), which show inverse square dependence of Q-factors on the asymmetric parameter. Far-field multiple decompositions and magnetic near-field enhancements further indicate that such two quasi-BICs are governed by MD responses, where asymmetric localized MD distributions in near-infrared wavelength realize indirectly manipulate the localized magnetic field. Further, multiple MDs with high Q-factors are designed as a multiwavelength sensor with a near theoretical FOM of ∼2300.

1 Introduction

Enhancing magnetic responses in all-dielectric nanostructures and metamaterials with high-refractive-index offer a powerful platform for efficient manipulation and localization of light at the nanoscale [1–3]. Magnetic dipole responses supported by all-dielectric metamaterials are particularly intriguing, as it can efficiently concentrate magnetic energy into subwavelength scales due to very low radiation loss compared with the electric dipole responses [4–6]. Various types of promising functions in dielectric nanostructures have been realized via involving MD responses, including enhanced magnetic nonlinearity [7], controllable light absorption [8], boosting MD transitions [9], dynamic nonlinear image [10] and directional scattering of light [11]. Therefore, how to fully exploit MD responses is extremely crucial for realizing and functionalizing the dielectric metamaterials.

Many mechanisms in dielectric metamaterials have been applied to enhance magnetic responses by minimizing the radiative loss including using trapped mode [12], Fano interference [13] and high-order modes [14], especially optical bound states in the continuum (BICs) [15–18], which make it possible to further improve the performance of magnetic responses in nanostructures. Ideal BIC in an optical system cannot directly be excited by incident wave and observed as a dark mode [19] due to infinitely long lifetime and infinitely high Q-factor, while quasi-BICs with finite lifetime and Q-factors allow the leakage of low radiation into free space and have been nicely observed in dielectric metamaterials [20–23]. Especially, the MD induced by quasi-BIC is known for its ability to boost the nonlinear process due to the associated string near-field enhancement and larger mode volume compared to other multipoles, which provide an approach to realize extreme light localization, nonlinear optical effects and radiation engineering [8, 10, 24, 25].

Recently, quasi-BICs allow small radiative leakage which results in finite but high Q-factors and can be realized by tuning structural symmetry and excitation parameters to distort the original ideal BICs [26–28]. Magnetic responses are highly dependent on the geometry of dielectric nanostructures, which broadens the horizon to manipulate MD responses induced by quasi-BICs by introducing geometric asymmetry [10, 24, 25, 29]. More importantly, magnetic responses are also highly dependent on choice of the structure's material, such as the permittivity or refractive index, offering an equally promising but a much less studied approach to control the MD quasi-BICs [30, 31].

In this work, we study multiple MD excitation supported by an all-dielectric metamaterial composed of permittivity-asymmetric nanodisk dimer. Through breaking permittivity symmetry in the nanodisk dimer,

[a] e-mail: wangm798@126.com
[b] e-mail: wangwd@dlpu.edu.cn (corresponding author)

symmetry-protected dual quasi-BICs with Fano line-shape can be observed in the transmission, whose Q-factors show the inverse quadratic dependence on asymmetry parameters. The calculated far-field contributions from multipole components and magnetic near-field distributions show the dominant multiple MD excitation, which preserve asymmetric magnetic confinement with large localized field enhancement. Further, multiple MDs with high Q-factors are designed as a multiwavelength sensor. Our work provides a useful insight into the multiple MD excitation induced by quasi-BICs in a permittivity-asymmetric all-dielectric metamaterial.

2 Structures description

Figure 1 shows the all-dielectric metamaterials of periodic nanodisk dimer embedded in a thin glass layer of thickness H. The lattice constant of the dimer unit cell is P. Geometric parameters of the dimer consist of the disk radius R and the gap width G. In our simulation, all transmission spectra are calculated by FDTD Solutions based on the finite-difference time-domain (FDTD) method, multipolar decomposition and near-field enhancement are calculated by COMSOL Multiphysics based on finite element methods, where periodical boundary conditions are set in the x and y directions, perfectly matched layers are set in the z direction and the x-polarized plane wave propagated along the z axis is normally incident on the structure. And we use the lossless silicon and glass with the permittivity ε_0 = 13.7 and ε_g = 1.94 in the calculation, respectively. The introduced permittivity-asymmetric ε can be realized by control the proportion of the silicon and doping impurities in the nanodisk. The asymmetric parameter $\delta = \sqrt{\varepsilon_0} - \sqrt{\varepsilon}$ is introduced to specify the structural asymmetry of unit cell.

3 Simulation results and discussions

Figure 2a shows the calculated transmission spectra at different δ. When the δ = 0.43, we can observe three modes marked as I, II, III, respectively. As the δ decreases, corresponding to decreasing the doping impurities, it can be seen that resonant wavelength of mode I slightly increases due to the increased effective refractive index of the dimer, while modes II and III undergo an obvious red shift and become sharper and finally vanish when the permittivity is symmetric (δ = 0), which confirms the existence of two symmetry-protected BIC states. Along with the permittivity asymmetry in the dimer, such two BIC states can be transformed into two quasi-BICs with Fano line-shape due to the interference between the free space continuum and discrete BIC states supported by dimer. This Fano line-shape can be fitted by a typical Fano formula given by [32]

$$T_{\mathrm{Fano}}(\omega) = \left| a_1 + ia_2 + \frac{b}{\omega - \omega_0 + i\gamma} \right|^2 \tag{1}$$

where a_1, a_2 and b are constant real numbers, γ is the overall damping rate and ω_0 is the central resonant frequency of the mode. And the Q-factor Q_{rad} of the mode can be extracted by $Q_{\mathrm{rad}} = \omega_0/2\gamma$. The fitted results for the δ = 0.43 are shown in Fig. 2(b). The Q-factors of mode I at 1734 nm, mode II at 1651 nm, mode III at 1552.7 nm reach 2357, 462 and 11,930, respectively. Figure 2c and d shows the extracted Q-factors of modes II and III at different δ. The Q-factors for the mode II and III exhibits the inverse quadratic trend and diverges as the δ approaches 0, which demonstrates that such two modes are indeed BICs.

Figure 3 shows the far-field scattered powers of the induced electric dipole, magnetic dipole, toroidal dipole, electric quadrupole and magnetic quadrupole moments based on the displacement current density under the Cartesian coordinate,

$$\vec{P} = \frac{1}{i\omega} \int \vec{j}\, d^3r, \tag{2}$$

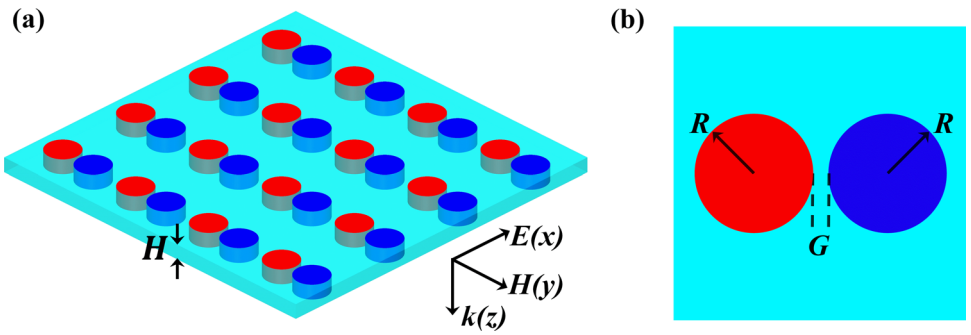

Fig. 1 **a** Schematic of all-dielectric metamaterials of nanodisk dimer embedded in a thin glass layer of thickness H. **b** Top-view cross section of the unit cell and definition of the geometrical parameters of the dimer. The structural symmetry is broken by introducing different permittivities in the dimer

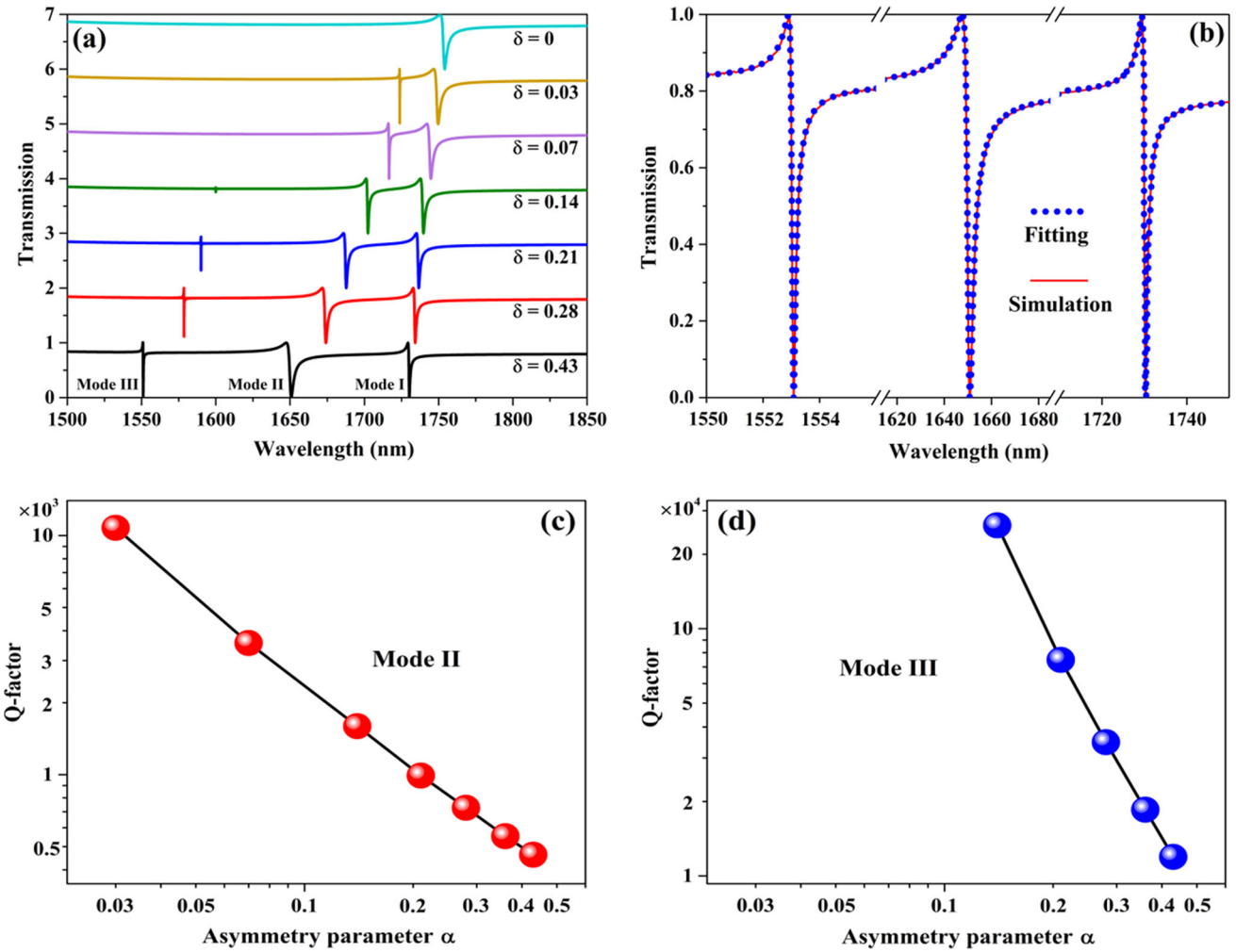

Fig. 2 **a** Evolution of simulated transmission spectra versus the δ changing from 0 to 0.43. Three modes are marked by I, II and III, respectively. Structural parameters: $R = 230$ nm, $T = 200$ nm, $G = 40$ nm, $P_x = P_y = 1200$ nm. **b** Fano fitted spectrum near the three modes for the $\delta = 0.43$. (**c**, **d**) Dependence of Q-factors on the δ for the mode II and mode III, respectively

$$\overrightarrow{M} = \frac{1}{2c}\int(\overrightarrow{r} \times \overrightarrow{j})d^3r, \tag{3}$$

$$\overrightarrow{T} = \frac{1}{10c}\int[(\overrightarrow{r} \cdot \overrightarrow{j})\overrightarrow{r} - 2r^2\overrightarrow{j}]d^3r, \tag{4}$$

$$Q^{(e)}_{\alpha\beta} = \frac{1}{2i\omega}\int[r_\alpha j_\beta + r_\beta j_\alpha - \frac{2}{3}(\overrightarrow{r} \cdot \overrightarrow{j})\delta_{\alpha\beta}]d^3r, \tag{5}$$

$$Q^{(m)}_{\alpha\beta} = \frac{1}{3c}\int[(\overrightarrow{r} \times \overrightarrow{j})_\alpha r_\beta + (\overrightarrow{r} \times \overrightarrow{j})_\beta r_\alpha]d^3r, \tag{6}$$

where c is the speed of light in a vacuum and the subscript $\alpha, \beta = x, y, z$ [33]. The $\overrightarrow{\mathrm{P}}$, $\overrightarrow{\mathrm{M}}$, $\overrightarrow{\mathrm{T}}$, $\overrightarrow{Q}^{(e)}$ and $\overrightarrow{Q}^{(m)}$ are the electric dipole (ED), magnetic dipole (MD), toroidal dipole (TD), electric quadrupole (EQ) and magnetic quadrupole (MQ) moments, respectively, and the corresponding scattered power is calculated by $I_P = \frac{2\omega^4}{3c^3}\left|\overrightarrow{\mathrm{P}}\right|^2$, $I_M = \frac{2\omega^4}{3c^3}\left|\overrightarrow{\mathrm{M}}\right|^2$, $I_T = \frac{2\omega^6}{3c^5}\left|\overrightarrow{\mathrm{T}}\right|^2$, $I_{Q^{(e)}} = \frac{\omega^6}{5c^5}\sum\left|\overrightarrow{Q}^{(\mathrm{e})}_{\alpha\beta}\right|^2$ and $I_{Q^{(m)}} = \frac{\omega^6}{40c^5}\sum\left|\overrightarrow{Q}^{(\mathrm{e})}_{\alpha\beta}\right|^2$, respectively. For mode I in Fig. 3a, the TD moment plays a dominant role at 1758 nm in comparison with other multipoles when the $\delta = 0$, while the MD moment is the strongest contributor for the mode I in Fig. 3b due to the introduced permittivity asymmetry when the $\delta = 0.43$. For mode II and III, MD contribution dominates across the wavelength region when the $\delta = 0.43$. This further confirms multiple MD excitation in permittivity-asymmetric all-dielectric metamaterials.

The dominant contributions of three MD modes can also be verified in magnetic near-field enhancement at resonant wavelengths in Fig. 4. The dominant TD moment in mode I manifests itself in the symmetric near-field distribution in Fig. 4a, where the magnetic field can be firmly constrained within the dimer and no

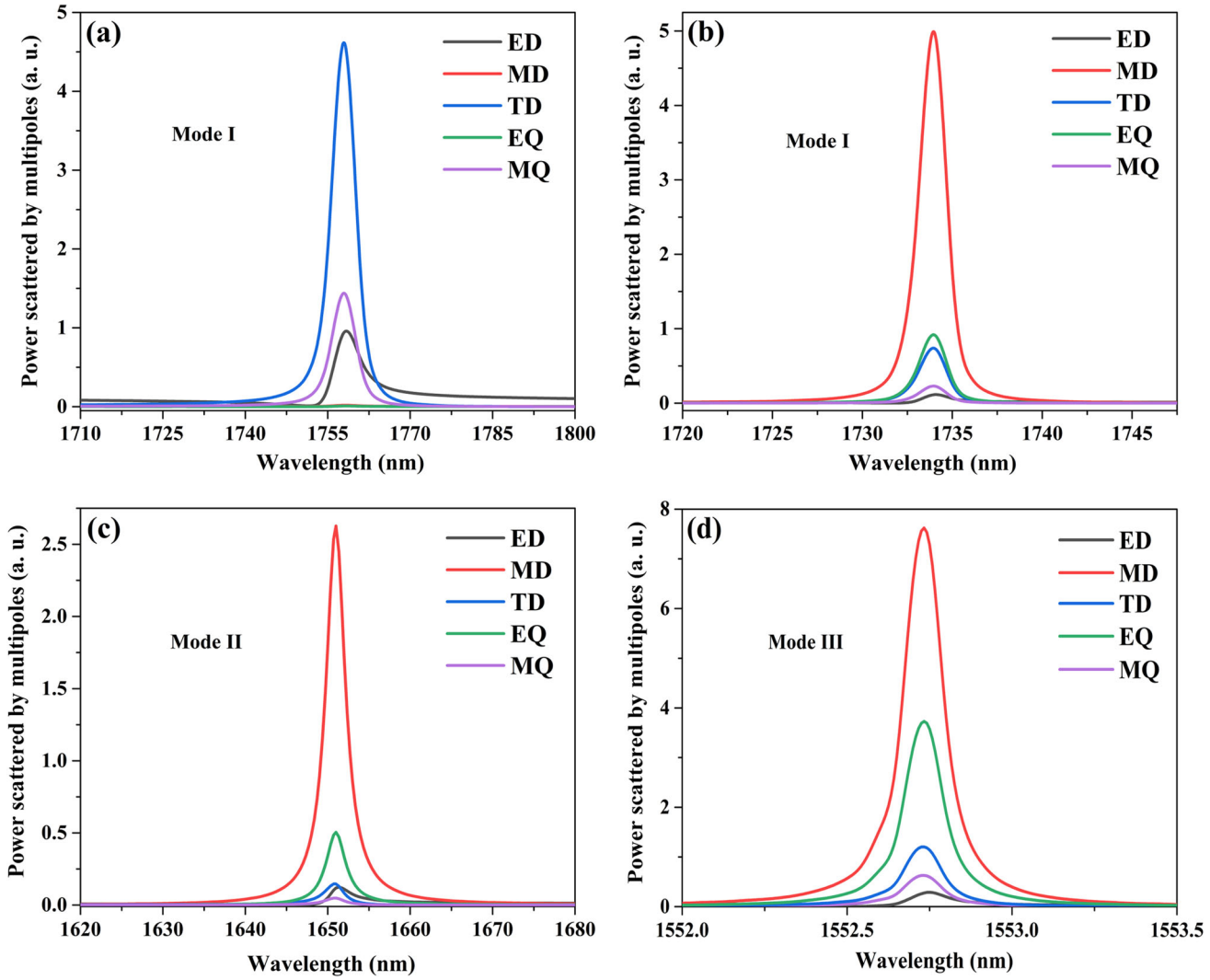

Fig. 3 Scattered powers of the Cartesian ED, MD, TD, EQ, and MQ for mode I at **a** $\delta = 0$ and **b** $\delta = 0.43$, respectively. (**c**, **d**) mode II and III at $\delta = 0.43$

radiation energy transmits outward at 1758 nm, and the electric field in the x–y plane forms two peculiar reversed loops, indicating a typical TD feature. However, asymmetric magnetic field enhancement in mode I is excited in Fig. 4b due to the introduced permittivity asymmetry when the $\delta = 0.43$. The asymmetric MD here is mainly aligned with the longitudinal direction (z-axis) and confined in the nanodisk with the high permittivity ($\varepsilon_0 = 13.7$). On the other hand, the dominant asymmetric magnetic near-field enhancement in mode III is mainly confined in the nanodisk with the low permittivity ($\varepsilon = 10.7$) in Fig. 4d. For mode II, the dominant MD enhancement in Fig. 4c is mainly localized in the nanodisk with the low permittivity ($\varepsilon = 10.7$), while weak TD moment is excited and confined in the nanodisk with the high permittivity ($\varepsilon_0 = 13.7$). It should be noted that MD moments in three modes cannot radiate along the z direction and radiation in the x–y plane can be ignored due to the array effect, which results in high Q-factors of multiple MD modes.

Figure 5a shows the calculated transmission spectra when the nanodisk dimer metamaterials ($\delta = 0.43$) are immersed in different refractive index of gaseous medium from 1.00 to 1.06. Thanks to high Q-factors of the three modes, transmission spectra show a remarkable red shift for modes I, II and III, even though a small refractive index fluctuation ($\Delta n = 0.02$). To have a detailed view of this trend, the shift of extracted resonant wavelengths $\Delta\lambda$ corresponding to the different refractive indices n is shown in Fig. 5b, where the fitted lines show a good linearity. The sensitivity (S) and figure of merit (FoM) are calculated as

$$S_\lambda(n) = \frac{\Delta\lambda}{\Delta n} \tag{7}$$

$$\mathrm{FoM}(n) = \frac{S_\lambda(n)}{\mathrm{FWHM}(n)} \tag{8}$$

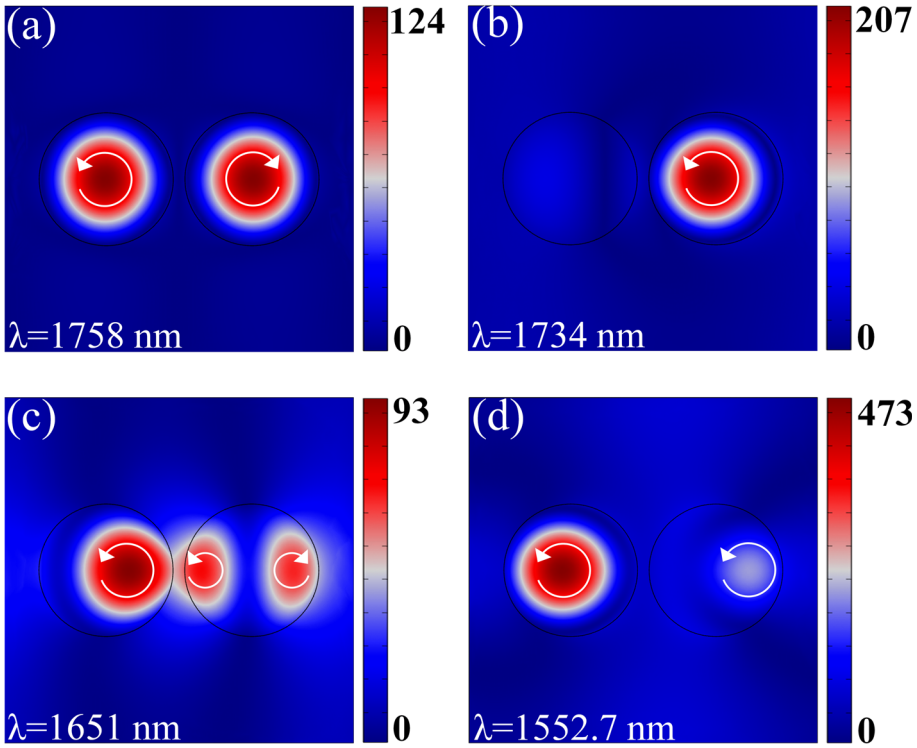

Fig. 4 Normalized magnetic field amplitudes $|H/H_0|$ in the middle x–y plane of the nanodisk dimer for different modes. **a** Mode I for the $\delta = 0$. (**b**–**d**) Modes I, II, III for the $\delta = 0.43$. White arrows show the electric field directions

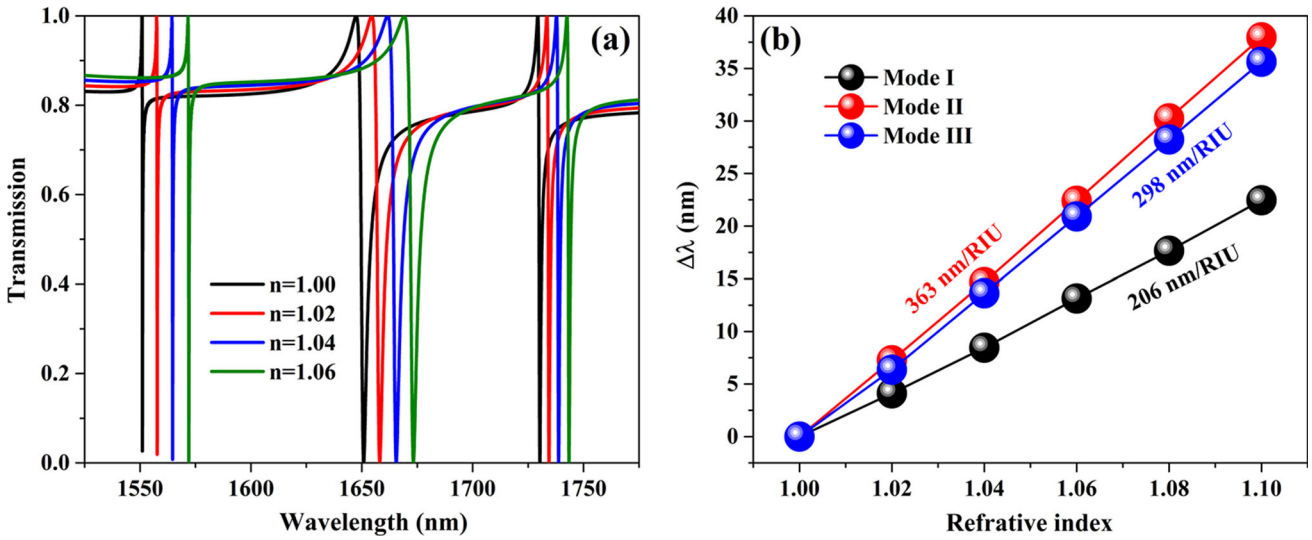

Fig. 5 **a** Transmission spectra of the proposed metamaterials ($\delta = 0.43$) for gaseous medium with different refractive index n. **b** Wavelength shifts as a function of the refractive index n

where FWHM is the full width at half maximum of mode [34]. As shown in Fig. 5b, the theoretical bulk refractive index sensitivity $S_\lambda(n)$ for modes I, II and III reaches 206, 363 and 298 nm/RIU, respectively. It is noteworthy that the sensitivity of modes II and III is higher than that of mode I due to the properties of quasi-BICs. Given the line width of the modes, the corresponding FoM of modes I, II and III reaches 229, 108 and 2292, respectively. Compared with the sensitivity with other published papers, the proposed metamaterial with high sensitivity and FoM shows its great superiority in multiwavelength biosensing application over the previous works [35–38] and can modify lines at several spectral positions simultaneously.

4 Conclusions

In conclusion, we have shown that multiple magnetic dipole excitation can be realized in an all-dielectric metamaterial composed of permittivity-asymmetric

nanodisk dimer with symmetric geometric parameters. In addition to the original MD mode, symmetry-protected dual quasi-BICs induced by introducing the permittivity asymmetry in the nanodisk dimer are observed and their Q-factors show inverse square dependence on the asymmetric parameter. The calculating far-field radiations and magnetic near-field distributions explicate the dominant multiple MD excitation in the metamaterials. Finally, the sensing characteristics of multiple MD modes are analyzed. This in-depth analysis of multiple MD excitation in permittivity-asymmetric all-dielectric metamaterials induced by quasi-BICs may facilitate the realization of efficient light–matter interaction with better performance.

Acknowledgements This work was supported by Natural Science Foundation of Liaoning Province (2019-ZD-0124, 64194902), National Natural Science Foundation of China (11647102) and Higher Education Key Program of Henan Province of China (No. 19A140014).

Author contribution

All authors contributed to the study conception and design. Material preparation, data collection and analysis were performed by Wudeng Wang. The first draft of the manuscript was written by Meng Wang and all authors commented on previous versions of the manuscript. All authors read and approved the final manuscript.

Data Availability Statement This manuscript has no associated data or the data will not be deposited. [Authors' comment: The datasets generated during and/or analyzed during the current study are available from the corresponding author on reasonable request.]

References

1. R.M. Bakker, D. Permyakov, Y. Kivshar, B. Lukyanchuk, A.I. Kuznetsov, Magnetic and Electric Hotspots with Silicon Nanodimers. Nano Lett. **15**(3), 2137–2142 (2015)
2. A.K. Ospanova, I.V. Stenishchev, A.A. Basharin, Anapole mode sustaining silicon metamaterials in visible spectral range. Laser Photonics Rev. **12**, 1800005 (2018)
3. W.D. Wang, L. Zheng, J.G. Qi, High Q-factor multiple Fano resonances for high-sensitivity sensing in alldielectric nanocylinder dimer metamaterials. Appl. Phys. Express **12**, 075002 (2019)
4. W.D. Wang, X. Zhao, L. Xiong, L. Zheng, Broken symmetry theta-shaped dielectric arrays for a high Q-factor Fano resonance with anapole excitation and magnetic field tunability. OSA Continuum **2**, 507–517 (2019)
5. A.B. Evlyukhin, S.M. Novikov, U. Zywietz, R.L. Eriksen, C. Reinhardt, S.I. Bozhevolnyi, B.N. Chichkov, Demonstration of magnetic dipole resonances of dielectric nanospheres in the visible region. Nano Lett. **12**, 3749–3755 (2012)
6. O. Tsilipakos, A.C. Tasolamprou, T. Koschny, M. Kafesaki, E.N. Economou, C.M. Soukoulis, Pairing toroidal and magnetic dipole resonances in elliptic dielectric rod metasurfaces for reconfigurable wavefront manipulation in reflection. Adv. Optical Mater. **6**, 1800633 (2018)
7. M. Shcherbakov, D.N. Neshev, B. Hopkins, A. Shorokhov, I. Staude, E. Melik-Gaykazyan, M. Decker, A. Ezhov, A.E. Miroshnichenko, I. Brener, Y.S. Kivshar, Enhanced third-harmonic generation in silicon nanoparticles driven by magnetic response. Nano Lett. **14**(11), 6488 (2014)
8. X. Wang, J.Y. Duan, W.Y. Chen, C.B. Zhou, T.T. Liu, S.Y. Xiao, Controlling light absorption of graphene at critical coupling through magnetic dipole quasi-bound states in the continuum resonance. Phys. Rev. B **102**, 155432 (2020)
9. C.M. Dodson, R. Zia, Magnetic dipole and electric quadrupole transitions in the trivalent lanthanide series: calculated emission rates and oscillator strengths. Phys. Rev. B **86**, 125102 (2012)
10. L. Xu, K.Z. Kamali, L.J. Huang, M. Woolley, D. Neshev, A.E. Miroshnichenko, Dynamic nonlinear image tuning through magnetic dipole quasi-BIC ultrathin resonators. Adv. Sci. **6**, 1802119 (2019)
11. J.H. Yan, P. Liu, Z.Y. Lin, H. Wang, H.J. Chen, C.X. Wang, G.W. Yang, Magnetically induced forward scattering at visible wavelengths in silicon nanosphere oligomers. Nat. Commun. **6**, 7042 (2015)
12. G.Q. Zhang, C.W. Lan, R. Gao, J. Zhou, Trapped-mode-induced giant magnetic field enhancement in all-dielectric metasurfaces. J. Phys. Chem. C **123**, 28887–28892 (2019)
13. S. Campione, S. Liu, L.I. Basilio, G.A. Keeler, I. Brener, M.B. Sinclair, Broken symmetry dielectric resonators for high quality factor Fano metasurfaces. ACS Photonics **3**(12), 2362–2367 (2016)
14. M.V. Rybin, K.L. Koshelev, Z.F. Sadrieva, K.B. Samusev, A.A. Bogdanov, M.F. Limonov, Y.S. Kivshar, High-Q supercavity modes in subwavelength dielectric resonators. Phys. Rev. Lett. **119**(24), 243901 (2017)
15. K. Koshelev, A. Bogdanov, Y. Kivshar, Meta-optics and bound states in the continuum. Sci. Bull. **64**(12), 836–842 (2019)
16. M.V. Gorkunov, A.A. Antonov, Y.S. Kivshar, Metasurfaces with maximum chirality empowered by bound states in the continuum. Phys. Rev. Lett. **125**, 093903 (2020)
17. K. Koshelev, S. Lepeshov, M. Liu, A. Bogdanov, Y. Kivshar, Asymmetric metasurfaces with high-Q resonances governed by bound states in the continuum. Phys. Rev. Lett. **121**(19), 193903 (2018)
18. C.W. Hsu, B. Zhen, A.D. Stone, J.D. Joannopoulos, M. Soljačić, Bound states in the continuum. Nat. Rev. Mater. **1**(9), 1–13 (2016)
19. E. Bulgakov, A. Sadreev, Formation of bound states in the continuum for a quantum dot with variable width. Phys. Rev. B Condens. Matter **83**, 1–9 (2011)
20. A.S. Kupriianov, Y. Xu, A. Sayanskiy, V. Dmitriev, Y.S. Kivshar, V.R. Tuz, Metasurface engineering through

bound states in the continuum. Phys. Rev. Applied **12**, 014024 (2019)
21. D.R. Abujetas, N. Barreda, F. Moreno, A. Litman, J.M. Geffrin, J.A. Sánchez-Gil, High-Q transparency band in all-dielectric metasurfaces induced by a quasi-bound state in the continuum. Laser Photonics Rev. **15**(1), 2000263 (2020)
22. Y. He, G.T. Guo, T.H. Feng, Y. Xu, A.E. Miroshnichenko, Toroidal dipole bound states in the continuum. Phys. Rev. B **98**(16), 161112 (2018)
23. S.Y. Li, C.B. Zhou, T.T. Liu, S.Y. Xiao, Symmetry-protected bound states in the continuum supported by all-dielectric metasurfaces. Phys. Rev. A **100**, 063803 (2019)
24. G.C. Yang, S.U. Dev, M.S. Allen, J.W. Allen, H. Harutyunyan, Optical Bound states in the continuum enabled by magnetic resonances coupled to a mirror. Nano Lett. **22**(5), 2001–2008 (2022)
25. S. Murai, D.R. Abujetas, G.W. Castellanos, J.A. Sánchez-Gil, F. Zhang, J.G. Rivas, Bound states in the continuum in the visible emerging from out-of-plane magnetic dipoles. ACS Photonics **7**(8), 2204–2210 (2020)
26. R.H. Chai, W.W. Liu, Z.C. Li, H. Cheng, J.G. Tian, S.Q. Chen, Multiband quasibound states in the continuum engineered by space-group-invariant metasurfaces. Phys. Rev. B **104**, 075149 (2021)
27. J.C. Jin, X.F. Yin, L.F. Ni, M. Soljačić, B. Zhen, C. Peng, Topologically enabled ultrahigh-q guided resonances robust to out-of-plane scattering". Nature London **574**, 501 (2019)
28. M.K. Liu, D.Y. Choi, Extreme Huygens' metasurfaces based on quasi-bound states in the continuum. Nano. Lett. **18**, 8062 (2018)
29. J.Y. Tian, Q. Li, P.A. Belov, R.K. Sinha, W.P. Qian, M. Qiu, High-Q all-dielectric metasurface: super and suppressed optical absorption. ACS Photonics **7**(6), 1436–1443 (2020)
30. S.L. Yu, Y.S. Wang, H. Li, S.Z. Song, T.G. Zhao, Dual-band polarization-insensitive toroidal dipole quasi-bound states in the continuum in a permittivity-asymmetric all-dielectric meta-surface. Opt. Express **30**(3), 4084–4095 (2022)
31. X. Liu, J. Li, Q. Zhang, Y. Wang, Dual-toroidal dipole excitation on permittivity-asymmetric dielectric metasurfaces. Opt. Lett. **45**(10), 2826–2829 (2020)
32. Y. Yang, I.I. Kravchenko, D.P. Briggs, J. Valentine, All-dielectric metasurface analogue of electromagnetically induced transparency. Nat. Commun. **5**(1), 5753 (2014)
33. N. Papasimakis, V.A. Fedotov, V. Savinov, T.A. Raybould, N.I. Zheludev, Electromagnetic toroidal excitations in matter and free space. Nat. Mater. **15**(3), 263–271 (2016)
34. C.B. Liu, Y. Bai, J. Zhou, J.H. Chen, L.J. Qiao, Refractive index sensing by asymmetric dielectric gratings with both bound states in the continuum and guided mode resonances. Opt. Express **29**, 42978–42988 (2021)
35. D.N. Maksimov, V.S. Gerasimov, S. Romano, S.P. Polyutov, Refractive index sensing with optical bound states in the continuum. Opt. Express **28**, 38907–38916 (2020)
36. S. Romano, G. Zito, S. Torino, G. Calafiore, E. Penzo, G. Coppola, S. Cabrini, I. Rendina, V. Mocella, Label-free sensing of ultralow-weight molecules with all-dielectric metasurfaces supporting bound states in the continuum. Photon. Res. **6**, 726–733 (2018)
37. S. Romano, G. Zito, S. Cabrini, E. Penzo, G. Coppola, I. Rendina, V. Mocellaark, Tuning the exponential sensitivity of a bound-state-in-continuum optical sensor. Opt. Express **27**, 18776–18786 (2019)
38. Y. Liu, W. Zhou, Y. Sun, Optical refractive index sensing based on high-Q bound states in the continuum in free-space coupled photonic crystal slabs. Sensors **17**(8), 1861 (2017)